Available online at www.sciencedirect.com
SCIENCE DIRECT
Journal of Sound and Vibration 295 (2006) 60–75
JOURNAL OF SOUND AND VIBRATION
www.elsevier.com/locate/jsvi

An investigation into the passive acoustic effect of the turbine in an automotive turbocharger

K.S. Peat[a,*], A.J. Torregrosa[b], A. Broatch[b], T. Fernández[b]

[a]*Department of Aeronautical & Automotive Engineering, Loughborough University, Loughborough, Leics LE11 3TU, UK*
[b]*CMT—Motores Térmicos, Universidad Politécnica de Valencia Camino de Vera, s/n-46022 Valencia, Spain*

Received 2 August 2004; received in revised form 21 November 2005; accepted 29 November 2005
Available online 17 April 2006

Abstract

The turbine of an automotive turbocharger is one of many elements in the exhaust line which lie between the primary noise source, namely the gas pulsations through the exhaust valves, and the primary noise radiation element, the exhaust tailpipe orifice. Like every other element of the exhaust system, it has a passive acoustic effect on the propagation of the primary exhaust noise. Thus knowledge of the passive acoustic effect of the turbine is essential to an understanding of the overall acoustic effectiveness of an exhaust system. In particular, if a comprehensive model of the acoustic propagation through the entire exhaust system of a turbocharged engine is sought, an acoustic model of the turbine is a prerequisite. This paper presents such a model as well as an experimental technique from which measured data can be obtained to verify the model and to characterise the acoustic behaviour of the turbine in a more general sense. In the first instance, the one-dimensional nonlinear equations of the fluid flow are solved for steady flow, to determine the background conditions for acoustic propagation including the mean convective flow distribution. The nonlinear time-domain flow equations are then linearised and solved for a single frequency of sound. At low frequencies, there is good agreement between measured and predicted results. System resonances that are observed at high frequencies can also be explained by the model.

1. Introduction

To date, fluid mechanical models of turbochargers for automotive applications have concentrated upon predicting the effect of the turbocharger on the overall performance of the engine. This is not surprising, since it is the sole purpose for which a turbocharger is used. Many such models can be found in the literature, varying from simplistic steady-flow models to comprehensive pulse-flow models, see for example Refs. [1–5]. A common alternative to trying to predict the effect of the turbocharger is to use measured data in the form of turbo-compressor and turbine maps to account for the effect of the turbocharger within an overall engine performance model, see for example Ref. [6].

Although the purpose of the turbocharger is to increase the power output of a given engine, the presence of the turbine and compressor within the exhaust and intake system respectively affects the propagation of sound

*Corresponding author. Tel.: +1 509 227232; fax: +1 509 227275.
E-mail address: K.S.Peat@lboro.ac.uk (K.S. Peat).

0022-460X/$ - see front matter © 2006 Elsevier Ltd. All rights reserved.
doi:10.1016/j.jsv.2005.11.033

through these systems. Thus in order to predict the acoustic performance of the entire exhaust or intake system on a turbocharged engine, at least a passive acoustic model of the turbine or turbo-compressor is required. The one-dimensional (1-D) pulse-flow models developed for engine performance prediction, as mentioned above, effectively include the acoustic performance, since in 1-D flow the fluid pulsations are the sound waves. However it is conventional in the modelling of the acoustic performance of exhaust and intake systems to make use of linear, plane-wave, frequency-domain analysis, since this simplified form of analysis enables one to model complex silencer configurations and produces accurate low-frequency results very efficiently [7–9]. The dominant sound in intake and exhaust systems occurs at engine firing frequency and its first few harmonics, within the low-frequency range for which the planar-wave assumption is valid. Although there are many similarities between the effect of the turbo-compressor in the intake system and the turbine in the exhaust system, this paper is restricted solely to consideration of the turbine.

To the best knowledge of the authors, this paper presents the first attempt to produce a linear acoustic model of the turbine of an automotive turbocharger. The turbine can be considered to be a noise source, but it only generates significant sound at very high frequencies associated with blade-passing. Thus attention here is focused upon the passive response of the turbine to the low- and mid-frequency acoustic waves, generated by the cylinder discharges, which propagate through the gas flow within the exhaust system.

Ideally, in order to experimentally characterise the passive acoustic effect of a turbine and to obtain results for validation of theoretical models, one would make measurements of the transmission loss across the turbine during normal on-engine operation of the turbocharger. Such measurements have been performed by the authors, despite the inherent difficulties of making accurate pressure measurements inside an exhaust pipe and maintaining constant controlled conditions of engine speed and operation. The main problem in these measurements was that the signal-to-noise ratio was only acceptable at the engine firing frequency and, sometimes, its first harmonic. Thus for a given engine operating condition, only measurements at one or two frequencies were reliable, which is insufficient for meaningful characterisation or model validation of the turbine. Hence an alternative experimental set-up for the turbine was developed in order to enable the operating conditions to be precisely controlled and to enable accurate measurements to be achieved across a broad spectrum of frequencies.

Section 2 of the paper describes this experimental rig, the measurement procedure and the results obtained for general characterisation of the passive acoustic effect of the turbine. Section 3 gives details of the nonlinear model for the mean flow and the linear acoustic model of the turbine. Section 4 compares measured and theoretical results for validation of the model.

2. Experimental set-up and measurements

Under normal operation within the exhaust line of an IC engine, the turbine is subject both to pressure pulses associated with cylinder discharge and to the resulting mean mass flow leaving the exhaust manifold. For this reason, in order to estimate the acoustical response of the turbine in conditions as close as possible to real operation, an experimental set-up based on the modified impulse method [10] with a superimposed mean flow was used in this work, so that both effects could be taken into account. In this test rig, the acoustical response of the turbine may be estimated in controlled conditions and with cold flow.

The effect of the turbine on exhaust acoustics arises mainly through two aspects: the transmission of the pressure perturbations coming from the engine, and the reflection at the turbine outlet of the perturbations coming from the exhaust line after reflection at the open end. In the usual terminology for acoustic sources, for a source located at the turbine outlet, one could say that the first aspect determines the source strength, whereas the second aspect is strongly related with the source impedance. Of course, reflection of pressure perturbations at the turbine inlet and transmission from the outlet to the inlet also play a role in the development of the acoustic field established, since these two processes may contribute significantly to the unsteady flow pattern upstream of the turbine and thus to the perturbations incident on the turbine.

In view of this physical picture, the transmission and reflection coefficients as seen from both sides of the turbine are required in order to present a global description of its acoustic behaviour. These two sets of coefficients may be similar when the element under study is symmetrical to some extent; however, in the case of the turbine one may not expect such symmetry, not only for geometrical or constructive reasons (different

inlet and outlet diameters, variable area passages, rotor blade design) but also for the fact that the mean flow (which is always present in real operation) defines a preferential direction and thus the system is intrinsically non-symmetric.

In summary, it is necessary to measure direct and inverse transmission and reflection coefficients, in the first case with the excitation travelling in the same direction as the mean flow, and in the second case in the opposite direction. The experimental set-up allowing for such measurements, together with an illustration of the measurement principle, is depicted in Fig. 1. Two main parts may be distinguished: the mean flow supply, and the pulse generation system and the ducting for pulse propagation and measurement. These two systems are described in the following.

The required steady air mass flow is supplied by a roots compressor driven by an electrical motor which is connected to the voltage source through a frequency converter. This arrangement allows the mass flow through the characterised element to be fixed by means of an automatic control process. A 30 l expansion chamber is located downstream of the compressor in order to reduce the pressure fluctuations generated by the blower. The stabilised mass flow is conveyed through a 110 mm diameter pipe up to a hot film anemometer, where the mass flow rate is measured. A 200 l volume is placed six diameters downstream of the anemometer in order to ensure stagnation conditions downstream of the flow meter. The volume outlet provides the last reflecting boundary to the pulse propagation within the ducting.

The rotational speed of the turbine is obtained from the energy provided by the mass flow generated in the volumetric compressor. This mass flow carries mainly kinetic energy, associated with the flow velocity, and very low enthalpy, since cold flow is being considered and the pressure rise generated by the roots compressor (in impulsion tests) is only as high as 100 kPa. Thus, the energy spent to drive turbine rotation comes basically from the kinetic side.

In order to allow for both direct and inverse tests, as will be further detailed below, the compressor was assembled in the set-up in such a way that both aspiration and impulsion tests could be performed. In any case, it should be noted that the electro-valve does not seal the corresponding end of the pipe, but the air is allowed to flow around the valve into or out of the rig as driven by the blower. The details in Fig. 1 shows the four ports drilled in the flange connecting the electro-valve to the propagation duct; the main considerations in

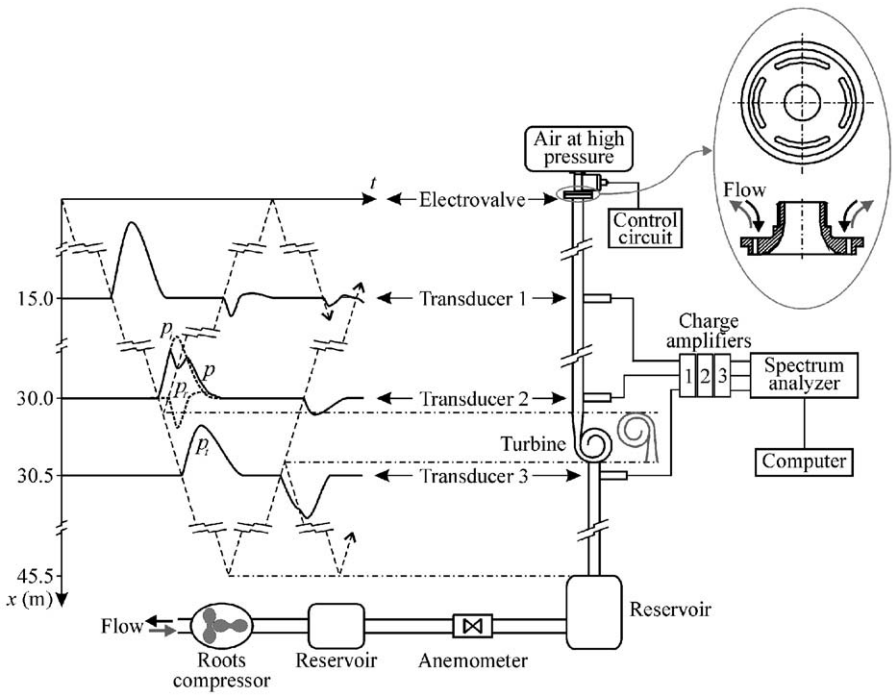

Fig. 1. Measurement principle and schematic of the experimental facility.

the design of these ports were related to the pressure drop generated, which should not be excessive for the blower, and the room available for different propagation duct diameters.

Regarding the pulse generation and propagation system, the turbine is excited by means of a pressure pulse generated by using an electro-valve that controls the discharge from a high-pressure reservoir. The amplitude and the duration of the pulse can be controlled by modifying the reservoir pressure and the opening time of the valve such that, after evolution of the pulse shape along the duct from nonlinear effects, a spectrum as flat as possible may be achieved, thus ensuring a proper excitation at all the frequencies of interest.

As the generated pulse propagates down the pipe (wave paths are indicated in Fig. 1 by dashed lines) instantaneous pressure is measured with piezoelectric transducers at three different points, as shown in Fig. 1: midway between the electro-valve and the turbine (transducer 1), just upstream of the turbine (transducer 2), and downstream of the turbine (transducer 3). The duct lengths between the valve and the first transducer and between the third transducer and the last reflecting boundary were chosen so as to enable the isolation of the pressure pulses in the time domain at transducers 1 and 3, as indicated by the wave propagation scheme in Fig. 1. In this way, the pressure recorded by transducer 3 gives directly the pulse p_t transmitted by the turbine. However, this choice of the lengths implies that, even with the weak nonlinearities to be expected with the pulse amplitudes considered, the waves recorded by transducer 1 cannot be directly used to extract information about the turbine. This issue is not determinant in the case of the incident pulse, since by the time it arrives at transducer 1 it has virtually reached its asymptotic "shock-wave" shape, but it is most critical in the case of the reflected pulse, which may suffer a noticeable distortion [10]. It is thus necessary to measure closer to the turbine, at a location such as that indicated for transducer 2 in Fig. 1. Obviously, this transducer records a pressure wave that is the result of the addition of the incident and the reflected pulses, as shown in the wave propagation scheme. However, the fact that the isolated incident pulse is available at the location of transducer 1 suggests the possibility to account for the propagation of this pulse up to the turbine inlet, so that the incident pulse upstream of the turbine (p_i in Fig. 1) could be determined. Then, from the measured pressure p and the estimated incident pulse p_i the reflected pulse p_r may be obtained. In principle, a nonlinear relation exists between p, p_i and p_r [11]; however, for the amplitudes considered in these experiments this relation can be linearised, so that p_r may be obtained, with good approximation, as

$$p_r = p - p_i. \tag{1}$$

All the magnitudes in Eq. (1) are indeed pressure fluctuations, as directly obtained from the piezoelectric transducers.

At this point, the only issue still to be addressed is the estimation of p_i from the incident pulse recorded by transducer 1. Since the propagation of the incident pulse over the long distance considered is intrinsically nonlinear, it is not possible to perform such estimation by a simple translation of the pulse recorded by transducer 1 to the new measurement station (transducer 2) or by applying any linear description of wave transfer between the two stations. To surpass this difficulty, the experimental solution chosen was to perform an additional test, in which the turbine is removed from the measurement set-up, so that the pressure pulse recorded by the transducer located at the position corresponding to the turbine inlet is thus p_i. It is imperative to ensure that the pulses generated by the valve in both tests, with and without the turbine, are comparable [10] in order to guarantee a suitable solution.

Finally, the resulting procedures for the direct and the reverse tests referred to above are also sketched in Fig. 1. For the direct test, the pulse excitation arrives at the turbine in the same direction as in real exhaust conditions. To move the rotor, in this case, air from the impulse test rig is aspirated by the Roots compressor (flow direction is indicated by black arrows), so that there is a certain vacuum at the turbine outlet. Reverse test are carried out by reversing the turbine within the rig (new disposition plotted in grey), such that pressure pulse first arrives at the outlet of the turbine. The Roots compressor is also reversed to work now in impulsion (flow direction indicated by grey arrows), so that the steady flow through the turbine still goes from inlet to outlet, but now in the direction opposite to that of the pulse.

The turbine used for the tests, which mounts a nine-blade rotor, is part of a small automotive turbocharger system. In order to simulate different working conditions, the rotation speed of the turbine rotor was varied. Due to limitations in the steady-flow supply, the maximum rotation speed obtained was 54,000 rev/min. Of course, this is lower than the rotation speed of the turbo-group in real engine operating conditions, but it was

expected that it would suffice to show the influence of the rotation on the acoustic response of the turbine. Tests with a rotation speed of 28,000 rev/min were also performed in order to check the sensitivity of the turbine response to a change in the rotor speed.

Apart from these, a test in which the turbine rotor was kept at a fixed position was also performed. While this configuration does not correspond to any realistic situation, it provides a limit condition which is interesting in two different senses: on one hand, it should provide a reference for the evaluation of the influence of rotation speed; on the other hand, the fact that no mean flow is present in such a test may give information about the influence of the mean flow on the quality of the measurements and thus on the reliability of the results obtained.

Primary results of the measurements are shown in Fig. 2, where the incident pulse estimated from the test without a turbine, the reflected pulse obtained from Eq. (1) and the transmitted pulse given by transducer 3 are plotted for both direct and reverse tests, and for the three rotor speeds considered (0, 28,000 and 54,000 rev/min). It can be observed that trends are quite different between direct and reverse tests. In direct tests, the

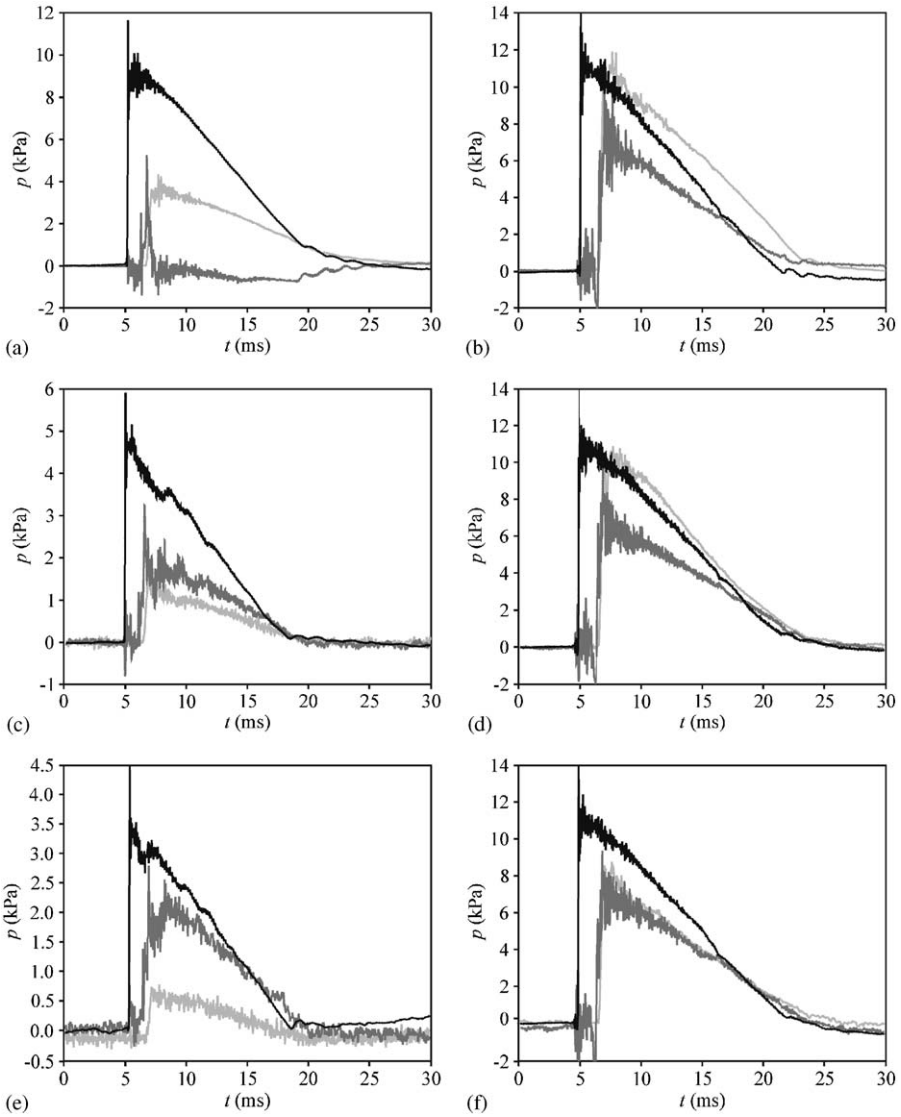

Fig. 2. Relevant pressure pulses: incident (black), reflected (dark grey) and transmitted (light grey). Rotor stopped: (a) direct, (b) inverse; 28,000 rev/min: (c) direct, (d) inverse; 54,000 rev/min: (e) direct, (f) inverse.

magnitude of the reflected and transmitted pulses relative to the magnitude of the incident pulse is strongly affected by rotation speed and/or the mean flow associated. In the case of the reflected pulse, there is even a change in the shape of the pulse between the case with fixed rotor (a sharp positive reflection followed by a weak rarefaction pulse) and the cases with moving rotor (in which only the positive reflection is observed). For transmitted pulses, a monotonic decrease of the relative amplitude is observed as rotational speed increases from zero. This behaviour of the transmitted pulses is also found in the reverse tests, although the influence is not so strong as in direct tests. However, in this case the reflected pulses are much less affected by rotational speed.

Another issue to be considered from Fig. 2 is the fact that, while in the reverse tests there is no significant influence of the mean flow on the incident pulse, this is not the case for direct tests. In fact, a reduction in the amplitude as well as a certain distortion in the pulse shape may be observed. These effects should be produced at pulse generation, due to the influence of the pressure drop across the valve on valve operation. In direct tests, one may expect a decrease in the local pressure downstream of the valve, so that the pressure drop across the valve is increased, whereas the opposite effect should be expected for reverse tests, in which an increase of the local pressure will occur. In both cases this is as a consequence of the restriction to the flow imposed by the flange ports. In this way, in direct tests the electro-valve is forced to work out of its design operational range.

The consequences of this issue on the requirements commented on above about the desirable characteristics of the incident spectrum are illustrated in Fig. 3, where the spectra of the incident pulses in both direct and reverse tests are plotted against the ratio of frequency f to the speed of sound in the unperturbed medium, $\bar{c}$. It is apparent that, while incident pulses for the reverse tests are fully comparable, there is a clear decrease in the level with increasing mean flow in the direct tests. Also, one may observe a certain distortion in the shape of the direct spectra, which is more apparent as mean flow increases, which can be attributed partly to the problems in valve operation as noted above, and partly to the decrease in the signal-to-noise ratio associated with the lower amplitudes found and the higher noise related with local turbulent fluctuations. While this must have some repercussion on the final results, there is still sufficient level in the incident pulses so as to provide significant information on the behaviour of the turbine.

From the Fourier analysis of the signals shown in Fig. 2, the reflection and transmission coefficients are directly obtained as a function of the frequency, from

$$R^D(f) = P_r^D(f)/P_i^D(f), \quad R^R(f) = P_r^R(f)/P_i^R(f), \tag{2}$$

$$T^D(f) = P_t^D(f)/P_i^D(f), \quad T^R(f) = P_t^R(f)/P_i^R(f). \tag{3}$$

Here P represents the complex amplitude of the pressure component, subscripts i, r and t refer to the incident, the reflected and the transmitted pulses, respectively, and superscripts D and R make reference to direct and reverse tests, respectively. It should be noted that any information regarding the influence of mean flow on wave propagation is already contained in these measured complex amplitudes. The latter does not hold, however, in the case of transmission loss, where acoustic power is involved, so that the Mach number of the

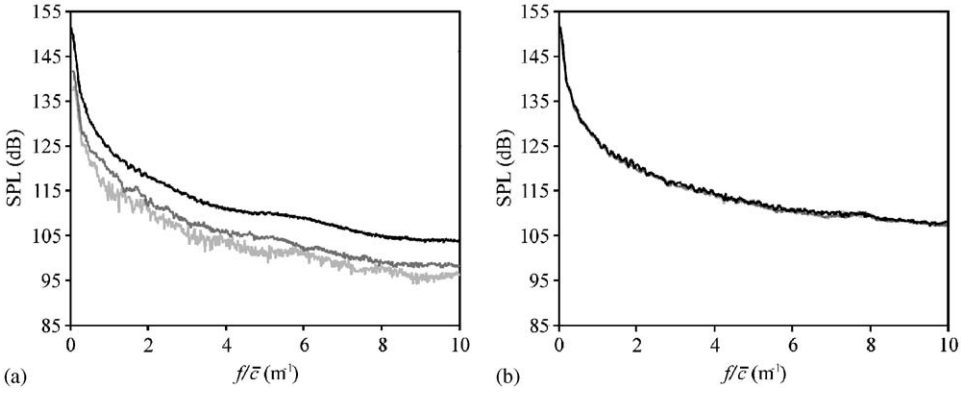

Fig. 3. Incident wave spectra: rotor stopped (black), 28,000 rev/min (dark grey) and 54,000 rev/min (light grey). Direct (a) and inverse (b).

mean flow must appear explicitly in the expression. For a simple wave with complex amplitude P travelling in the same direction as a mean flow with Mach number M, the acoustic power for sufficiently large Stokes and Reynolds numbers may be expressed, to a close approximation, as [12] $W = [|P|^2(1+M)^2]S/(\bar{\rho}\bar{c})$, where $\bar{\rho}$ is the density in the unperturbed medium and S represents the cross-sectional area of the duct. Therefore the transmission loss, defined as the ratio of the incident to the transmitted power, is given by

$$\begin{aligned} \mathrm{TL}^D(f) &= 20\log\left|1/T^D(f)\right| + 10\log(S_u/S_d) + 20\log\left|(1+M_u)/(1+M_d)\right|, \\ \mathrm{TL}^R(f) &= 20\log\left|1/T^R(f)\right| + 10\log(S_u/S_d) + 20\log\left|(1-M_u)/(1-M_d)\right|. \end{aligned} \tag{4}$$

Here, subscripts u and d refer to the upstream and downstream sections relative to wave propagation, respectively. In the direct tests, the upstream and downstream diameters were 33 and 51 mm, respectively, and the corresponding Mach numbers were $M_u = 0.05$ and $M_d = 0.028$ for 28,000 rev/min and $M_u = 0.078$ and $M_d = 0.043$ for 54,000 rev/min, so that the area term amounts to -3.8 dB, and the Mach number term to 0.18 and 0.28 dB, respectively; in the reverse tests, the area term is obviously 3.8 dB and the Mach numbers exchange roles, so that the corresponding terms are now 0.2 and 0.32 dB for 28,000 and 54,000 rev/min, respectively. As can be seen, the values of the mean flow terms are well within the experimental uncertainty and are thus neglected in the experimental results shown below.

In Fig. 4, results for reflection and transmission coefficients and transmission loss, in both direct and reverse tests, are plotted against the ratio of frequency to sound speed, $f/\bar{c}$. As a general comment, it can be observed that the results are affected by a certain ripple, which is more important as the mean flow (and consequently the rotational speed) increases. Moreover, this ripple is much more apparent in the direct tests, accordingly with the progressive degradation of the quality of the incident pulse spectrum observed in Fig. 3.

As could be expected in view of the pulses shown in Fig. 2, differences between the magnitudes measured under direct and reverse characterisation are evident. In the case of transmission coefficients, the shape is quite similar between direct and reverse, the frequencies associated with spikes and troughs being roughly the same, but the levels are quite different. However, in the case of the reflection coefficients both the shape and levels change. This is a consequence of the non-symmetric character of the turbine, and suggests that there is an internal strongly reflecting boundary, most likely related to the rotor, that decouples to some extent the inlet and the outlet of the turbine.

Regarding the influence of the rotor speed on the turbine behaviour, only relatively small effects can be observed, except in the very low frequency range, and mostly in the direct tests.

From the magnitudes depicted in Fig. 4, it is possible in principle to establish the acoustic power balance of the turbine, since incident, reflected and transmitted power can be estimated and, from the difference, eventual acoustic power dissipation or generation could be identified. However, under the required processing all the ripples present in the measured coefficients are magnified, so that it is difficult to extract precise conclusions, particularly regarding the eventual presence of noise generation. Even though these results are not shown here in view of their poor quality, it was possible at least to guess that dissipation/generation effects increase with the mean flow (and the rotational speed), as could be expected.

3. Turbine model

The turbine can be considered to comprise three separate sections, a volute, a rotor and a diffuser, see Fig. 5. In each section, one requires the equations of 1-D flow in the local flow direction x through a tube of varying cross-sectional area $A(x)$ and perimeter $l_P(x)$. The rotor consists of a number, say n, of identical curved blades with n flow passages between them. It is assumed for simplicity that the entire flow through the volute and diffuser is distributed evenly between the n rotor passages and that the local flow direction is that of the blades. Furthermore the real distributed effect of mass flow from the volute into each passage of the rotor is averaged, such that the total flow is assumed to leave the volute at a single axial location $x = x_h$ and to then divide equally between the n rotor passages, see Figs. 5 and 6. This location is taken to be half-way around the outer circumference of the rotor from the flow entry position. The cross-sectional area of the volute is kept artificially high over this distance to maintain the correct total volume of volute and flow velocity within it. Within the rotor, coordinate x is taken to rotate with the rotor at angular velocity Ω and the flow velocity V

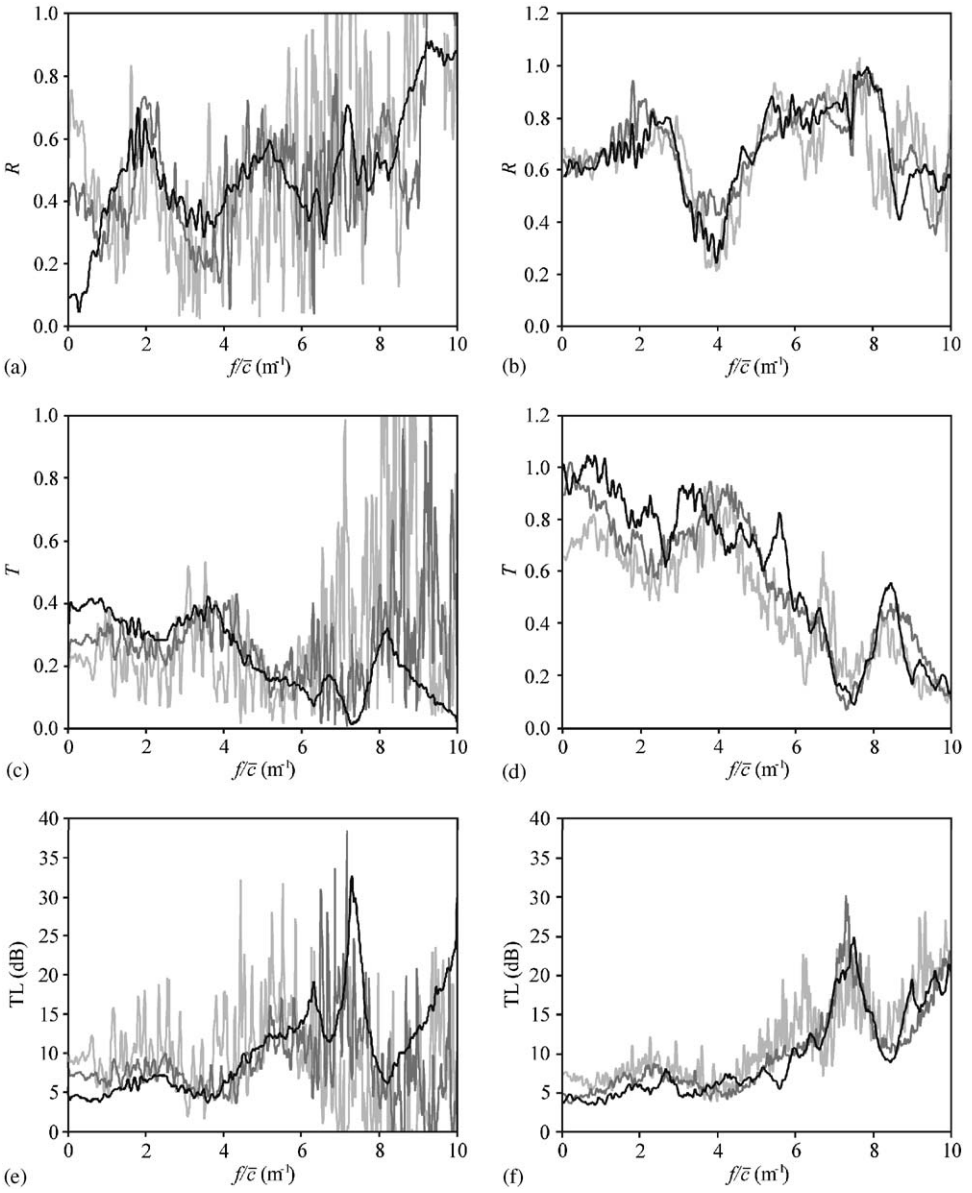

Fig. 4. Measurement results: rotor stopped (black), 28,000 rev/min (dark grey) and 54,000 rev/min (light grey). Reflection coefficient: (a) direct, (b) inverse; transmission coefficient: (c) direct, (d) inverse; transmission loss: (e) direct, (f) inverse.

here is taken to be the velocity relative to the rotor. The 1-D, nonlinear time-dependent equations of conservation of mass, momentum and energy pertinent to all three sections of the turbine can then be written as [4]

$$\frac{\partial}{\partial t}\begin{bmatrix}\rho\\ m\\ e\end{bmatrix}+\frac{\partial}{\partial x}\begin{bmatrix}m\\ mV+p\\ hV\end{bmatrix}=\begin{bmatrix}-\frac{m}{A}\frac{\mathrm{d}A}{\mathrm{d}x}\\ -\frac{mV}{A}\frac{\mathrm{d}A}{\mathrm{d}x}+\rho(B-F)\\ -\frac{hV}{A}\frac{\mathrm{d}A}{\mathrm{d}x}+mB\end{bmatrix}, \tag{5}$$

where ρ is the density, p is the pressure, $m=\rho V$, $e=\rho V^2/2+p/(\gamma-1)$, $h=e+p$, $F=\lambda l_P V^3/8A/|V|$ is the wall friction per unit volume and $B=\Omega^2 r\,\mathrm{d}r/\mathrm{d}x$. Here λ is the coefficient of friction, $r(x)$ is the radial distance of the

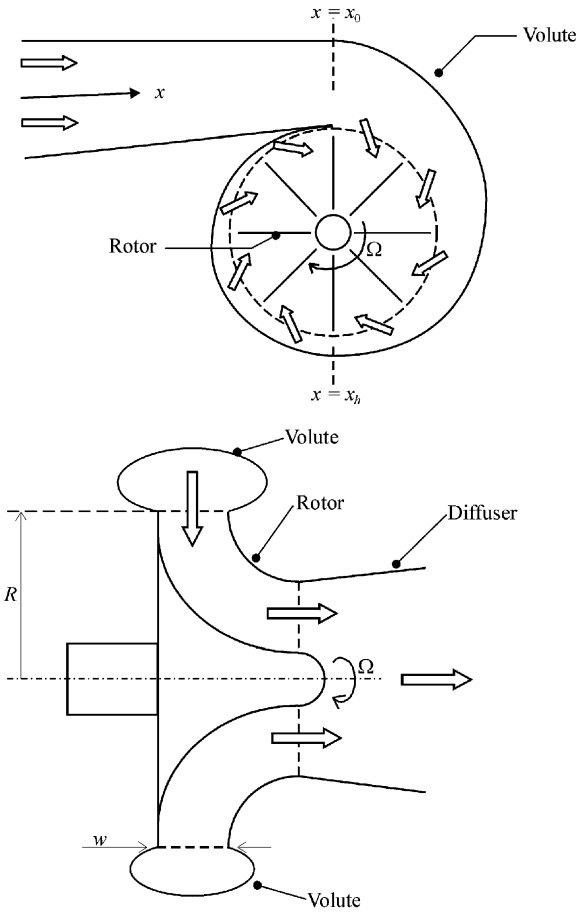

Fig. 5. Schematic of a turbine.

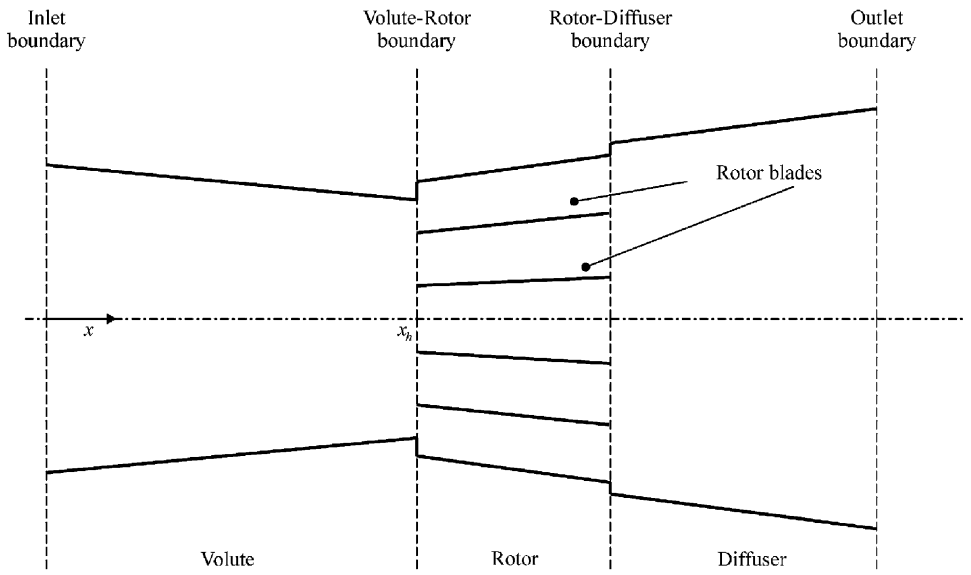

Fig. 6. Simplified geometry of the turbine for the model.

1-D flow line from the axis of rotation, and of course $B = 0$ in the volute and diffuser. When $B = 0$, Eqs. (5) revert to the usual equations of 1-D unsteady gas dynamics [13]. In the rotor section, where the streamwise coordinate x and velocity V are written with respect to a coordinate system that rotates with angular velocity Ω, the momentum and energy equations become modified by terms that account for the centripetal acceleration [14]. It is assumed throughout that the exhaust gas is a perfect gas.

3.1. Steady-flow analysis

In the first instance, steady-flow solutions to Eq. (5) are sought in order to determine the background fluid properties for all x, since these govern the propagation and convection of the sound waves. Let the steady-flow variables be denoted by overbars, such that $\rho = \overline{\rho}(x)$, etc. Eq. (5), with the time derivative set to zero, becomes a set of three coupled first-order nonlinear ordinary differential equations:

$$\frac{\mathrm{d}}{\mathrm{d}x}\begin{bmatrix} \overline{m} \\ \overline{m}\overline{V}+\overline{p} \\ \overline{h}\overline{V} \end{bmatrix} = \begin{bmatrix} -\frac{\overline{m}}{A}\frac{\mathrm{d}A}{\mathrm{d}x} \\ -\frac{\overline{m}\overline{V}}{A}\frac{\mathrm{d}A}{\mathrm{d}x}+\overline{\rho}(\overline{B}-\overline{F}) \\ -\frac{\overline{h}\overline{V}}{A}\frac{\mathrm{d}A}{\mathrm{d}x}+\overline{m}\overline{B} \end{bmatrix}, \tag{6}$$

where

$$\overline{B} = \overline{\Omega}^2 r\,\mathrm{d}r/\mathrm{d}x \text{ and } \overline{F} = \lambda l_P \overline{V}^3/8A/|\overline{V}|.$$

All geometrical data is assumed known, in particular $A(x)$ throughout the turbine and $r(x)$ through the rotor. Solution for the flow properties as a function of distance x throughout each section of the turbine then follows from use of a two-step, predictor-corrector forward finite difference scheme. Thus, if $\overline{m}_i$ is the known value of $\overline{m}$ at position $x_i = i\delta x$, etc., then for example the momentum Eq. 6(b) has a predictor step

$$(\overline{m}\overline{V}+\overline{p})^p_{i+1} = (\overline{m}\overline{V}+\overline{p})_i - \frac{\overline{m}_i\overline{V}_i}{A_{i+1/2}}(A_{i+1}-A_i) + \overline{\rho}_{i+1/2}(\overline{B}_{i+1/2}-\overline{F}_{i+1/2})\delta x \tag{7}$$

and a corrector step

$$(\overline{m}\overline{V}+\overline{p})_{i+1} = (\overline{m}\overline{V}+\overline{p})_i - \frac{\overline{m}^p_{i+1/2}\overline{V}^p_{i+1/2}}{A_{i+1/2}}(A_{i+1}-A_i) + \overline{\rho}^p_{i+1/2}\left(\overline{B}^p_{i+1/2}-\overline{F}^p_{i+1/2}\right)\delta x. \tag{8}$$

Here $A_{i+1/2} = (A_{i+1}+A_i)/2$, $\overline{m}^p_{i+1/2} = (\overline{m}^p_{i+1}+\overline{m}_i)/2$, etc. Once the three predictor or corrector steps for all three equations have been completed, values of the separate fluid properties must be determined from the updated values of $\overline{m}$, $(\overline{m}\overline{V}+\overline{p})$ and $\overline{h}\overline{V}$. Expansion of $\overline{h}$ and then elimination of $\overline{V}$ and $\overline{p}$ leaves a quadratic equation for the density

$$\left[(\overline{h}\overline{V}) - \frac{1}{2}\overline{m}(\overline{\Omega}r)^2\right]\overline{\rho}^2 - \left[\frac{\gamma}{\gamma-1}\overline{m}(\overline{m}\overline{V}+\overline{p}) - \overline{m}^2\overline{\Omega}r\right]\overline{\rho} + \left(\frac{\gamma}{\gamma-1}-\frac{1}{2}\right)\overline{m}^3 = 0. \tag{9}$$

It is a simple matter to choose the correct root of the quadratic, after which $\overline{V}$, $\overline{p}$ and $\overline{h}$ follow directly from each conservative variable in turn. As noted previously, the fluid is assumed to be a perfect gas, thus the steady-state temperature and hence speed of sound and Mach number at each position x_i can now readily be determined.

All the fluid properties at the inlet to the volute, $i = 0$, are assumed given, such that the complete solution follows from a marching procedure from i to $i+1$. Matching conditions at the volute–rotor and rotor–diffuser boundaries are also required in order to progress the solution from one section of the turbine to the next. At both boundaries, continuity of pressure, temperature and mass flow rate is enforced. Assume for the moment that at the volute–rotor boundary, the outlet flow angle from the volute, α, is known, see Fig. 7. This would be the case for a turbine with inlet guide vanes, since the outlet flow angle from the volute is governed by the guide vanes in normal operation. Thus the flow out of the volute occurs at angle α to an outlet slot of known radius and width, say R and w, see Fig. 5. The cross-sectional area normal to the flow direction at the outlet of the volute is then $Rw\sin(\alpha)$. It is assumed that the cross-sectional area of the equivalent volute varies linearly

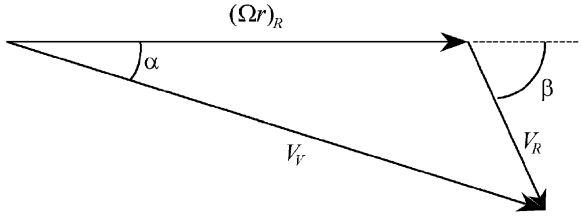

Fig. 7. Velocity vector diagram at the volute–rotor boundary.

from the known area at which the volute opens to the first rotor passage, at $x = x_o$, to this calculated outlet area at a distance $x = x_h$, see Fig. 5. Thus $A(x)$ is known throughout the equivalent volute, as previously assumed. Let the inlet angle of the stationary rotor blades be β, Fig. 7, and assume that the flow through the spinning rotor follows the blades. Now conservation of mass at the volute–rotor boundary implies

$$A_V \overline{V}_V = nA_R \overline{V}_R, \tag{10}$$

where subscripts V and R refer to the volute outlet and rotor inlet respectively. A_R is the cross-sectional area of a single rotor passage normal to the blades. This is sufficient to determine the inlet velocity to the rotor and then the rotor speed follows from the vector diagram of Fig. 7. Given that conservation of mass flow rate has been enforced, it is then clear from Fig. 7 that both axial and angular momentum are also conserved at the rotor inlet. Use of the constant temperature boundary condition gives rise to a small imbalance in the energy equation, because the correct condition to use is conservation of total enthalpy [4]. Use of the latter condition demands an iterative solution process and, since the results from using the simpler constant temperature condition showed negligible differences, this approximate condition was adopted.

The turbine tested within this piece of work did not have inlet guide vanes, such that the outlet flow angle, α, from the volute is unknown, but the turbine speed was measured. With α unknown, it is not possible to determine the cross-sectional area of the outlet flow from the equivalent volute and hence $A(x)$ throughout the volute. An iterative solution procedure was adopted to overcome this difficulty. A guess was made for α, such that an estimate of $A(x)$ could be made and then the flow properties throughout the volute followed. Thus the rotor speed could be evaluated as above and compared to the known rotor speed. The value of α was then adjusted and the process repeated until the rotor speed converged to the correct value.

In contrast to the volute–rotor boundary, matching conditions at the rotor–diffuser boundary follow simply from continuity of pressure, temperature and mass flow rate. If the swirl velocity is required at the rotor–diffuser boundary, to calculate the torque for example, it follows from a similar velocity vector diagram as given in Fig. 7.

It is possible to determine the overall performance parameters from such a steady-flow analysis, such as the torque and power output of the rotor. This has been done and the results have been compared with data from a comprehensive engine performance model that utilises the turbine and compressor maps [15]. The comparison was quite poor. However the changes in pressure and velocity across the turbine agreed well. Furthermore the predicted changes of pressure across the turbine agreed well with measured data, although the measured temperature drop across the turbine was greater than predicted. The only reason that a steady-flow analysis is required for the present work is to determine the fluid properties of the steady-flow with distance x through the turbine, in order to subsequently calculate the propagation of sound waves through this medium. In such a context, the accuracy requirements on the steady-flow data are not particularly high and therefore a simplified analysis of the form given above is more than adequate.

3.2. Acoustic analysis

Each fluid property of Eqs. (5) is written as the sum of a steady-flow value and an acoustic value, e.g. $\rho = \overline{\rho}(x) + \rho'(x, t)$. It is assumed that the acoustic disturbance is isentropic, i.e. $p' = \rho' \overline{c}^2$, which removes the requirement to consider the energy equation within Eqs. (5) in this section. The steady-flow equations are then

subtracted from the overall equations and the resulting equations are linearised on the basis that acoustic values are small enough for products of acoustic variables to be negligible in comparison to first-order terms. Once the equations are linearised it is sufficient to consider a single harmonic component of frequency ω say. Thus Eq. (5) reduce to

$$\begin{bmatrix} \overline{\rho}\,\overline{c} & \overline{M} \\ \overline{\rho}\,\overline{c}\,\overline{M} & 1 \end{bmatrix} \begin{bmatrix} \frac{\mathrm{d}V'}{\mathrm{d}x} \\ \frac{\mathrm{d}p'}{\mathrm{d}x} \end{bmatrix} = \begin{bmatrix} \mathrm{i}kp' - p'\frac{\mathrm{d}\overline{M}}{\mathrm{d}x} - V'\overline{c}\frac{\mathrm{d}\overline{\rho}}{\mathrm{d}x} - \left(\overline{M}p' + \overline{\rho}\,\overline{c}V'\right)\frac{1}{A}\frac{\mathrm{d}A}{\mathrm{d}x} \\ \mathrm{i}k\overline{\rho}\,\overline{c}V' - \left(\overline{M}p' + \overline{\rho}\,\overline{c}V'\right)\frac{\mathrm{d}\overline{M}}{\mathrm{d}x} + \left(\frac{\overline{\Omega}^2}{\overline{c}^2}p' + 2\overline{\rho}\overline{\Omega}\Omega'\right)r\frac{\mathrm{d}r}{\mathrm{d}x} \end{bmatrix}, \tag{11}$$

where $\overline{M} = \overline{V}/\overline{c}$ is the steady-flow Mach number and $k = \omega/\overline{c}$ is the wavenumber. It may be noted that the frictional term F in Eqs. (5) make no contribution to the linearised acoustic equations above, thus there is no concern in regard to the applicability of a quasi-steady-flow term to the acoustic equations.

Exactly the same geometrical data for the turbine is needed here as for the steady-flow analysis, and of course the steady-flow properties are now known. Thus one is left with a pair of coupled first-order differential equations to solve for the variation of acoustic pressure and velocity throughout the turbine. The equations are in fact solved twice, for two different sets of inlet boundary conditions, namely $\{p' = 1,\ V' = 0\}$ and $\{p' = 0,\ V' = 1\}$. Once again, in each case, solution is effected by means of a two-step, predictor–corrector forward finite difference scheme, with matching conditions at the volute–rotor and rotor–diffuser boundaries in order to progress the solution from one section of the turbine to the next. At both boundaries, continuity of acoustic pressure and acoustic mass flow rate is enforced. At the volute–rotor boundary, the outlet flow angle from the volute is assumed to be the same as for the steady-flow, whether or not the turbine has inlet guide vanes. The fluctuation in rotor speed Ω' then follows in a similar manner to the evaluation of $\overline{\Omega}$ as given for the steady-flow case.

Thus, for a given set of inlet conditions, the acoustic properties are evaluated throughout the turbine. In particular, they become known at the outlet section of the turbine. Let the overall transfer matrix that describes the acoustic effect of the turbine have four-pole parameters A, B, C, D such that

$$\begin{bmatrix} p'_{\mathrm{in}} \\ V'_{\mathrm{in}} \end{bmatrix} = \begin{bmatrix} A & B \\ C & D \end{bmatrix} \begin{bmatrix} p'_{\mathrm{out}} \\ V'_{\mathrm{out}} \end{bmatrix}. \tag{12}$$

The two separate numerical solutions from the two sets of inlet boundary conditions then enable one to determine the four-pole parameters A, B, C, D for a single frequency of sound since

$$\begin{bmatrix} 1 \\ 0 \end{bmatrix} = \begin{bmatrix} A & B \\ C & D \end{bmatrix} \begin{bmatrix} p'_{\mathrm{out}} \\ V'_{\mathrm{out}} \end{bmatrix}_1 \text{ and } \begin{bmatrix} 0 \\ 1 \end{bmatrix} = \begin{bmatrix} A & B \\ C & D \end{bmatrix} \begin{bmatrix} p'_{\mathrm{out}} \\ V'_{\mathrm{out}} \end{bmatrix}_2, \tag{13a,b}$$

where the subscript relates to the set of solution. The values of the acoustic variables at the outlet are given by the solutions, thus there are four equations from which to determine the four unknown four-pole coefficients. Once these are determined, any further acoustic property, e.g. transmission loss, follows simply [16].

4. Results

Comparison between measured and predicted transmission loss across the turbine at three different rotational speeds of the turbine is shown in Figs. 8–10. In each case two plots are shown, one for the direct case where the incident sound is in the flow direction and impinges first upon the volute, and the second is the reverse case where the incident sound is in the opposite direction to the flow and impinges first upon the diffuser. In each plot two curves of theoretical results are shown. Those marked 'Rotating' are a result of the model described in Section 3. In all cases they are accurate up to a frequency of around 1200 Hz, after which the predicted transmission loss is too low and does not feature the resonance peaks characteristic of the experimental results. The cut-on frequency of non-planar waves in the test set-up is over 5 kHz, as the cross-sectional area of the ductwork is small. Thus the errors cannot be attributed to failure of the plane-wave assumption. However, it should be noted that since these tests were conducted for cold flow, the corresponding maximum frequency of accurate prediction in the hot exhaust flow of normal operation would

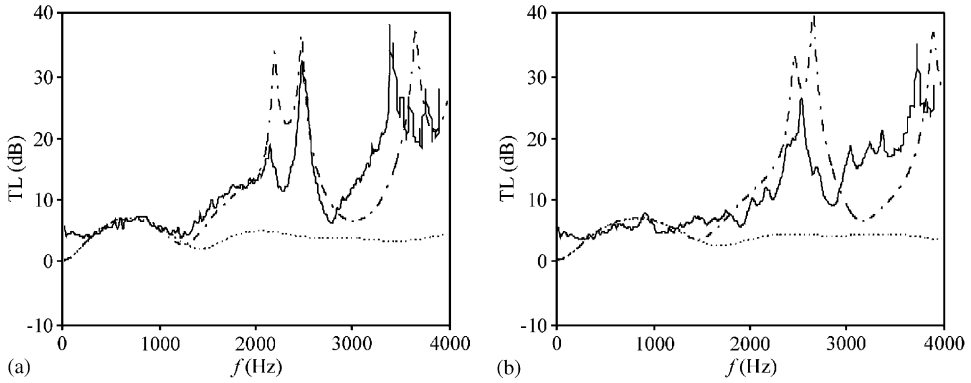

Fig. 8. Comparison of measured and predicted transmission loss of the turbine at a rotational speed of 0 rev/min (a) direct and (b) reverse. ——, experimental; - - - - - - -, rotating: averaged geometry model of the volute and rotor including rotational effects of the turbine (see Section 3); –·–·–·–, volume: distributed volute and rotor passage model excluding rotational effects of the turbine (see Section 4).

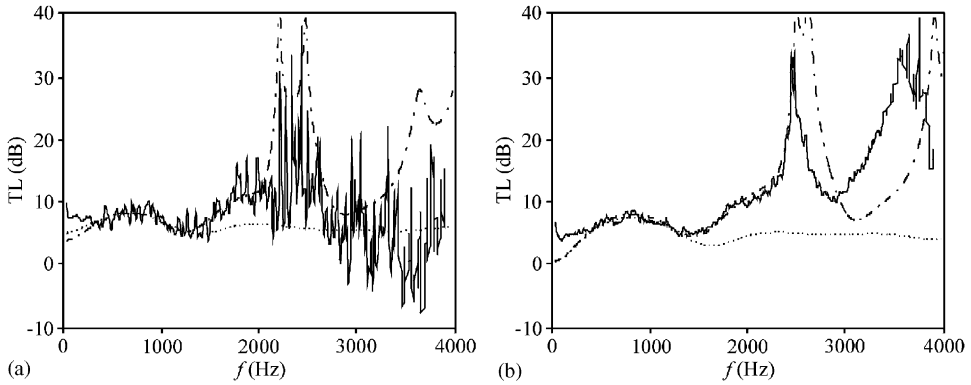

Fig. 9. Comparison of measured and predicted transmission loss of the turbine at a rotational speed of 28,000 rev/min (a) direct and (b) reverse. Key as Fig. 8.

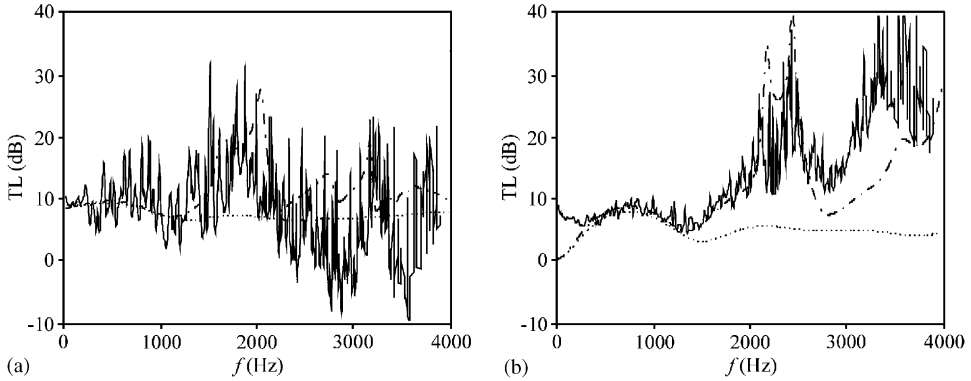

Fig. 10. Comparison of measured and predicted transmission loss of the turbine at a rotational speed of 54,000 rev/min (a) direct and (b) reverse. Key as Fig. 8.

be about 2 kHz. Since the cut-on frequency of non-planar waves in the complete silencer system of a road vehicle in normal operation is typically around 1 kHz, the model of Section 3 is quite sufficient to characterise the turbine as one acoustic element within a linear frequency domain model of the entire exhaust system.

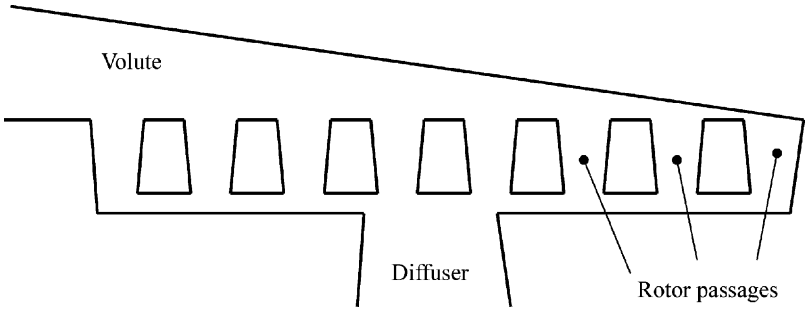

Fig. 11. Distributed static model of the volute and rotor.

It is of interest, however, to try and gain an understanding of the higher frequency characteristics of a turbine as seen in the experimental results, even for the case of zero rotational speed. In this regard, a static model of the turbine was created using standard linear acoustic elements of uniform pipes, conical pipes and area discontinuities [8,17]. Thus rotational effects of the turbine were completely ignored but the variation of the background fluid properties throughout the turbine, including the mean flow Mach number, was the same as for the full model with rotation, as given by the analysis of Section 3.1. The turbine geometry was initially modelled in precisely the same way as in Section 3, with an 'averaged' volute feeding into identical rotor passages at the same axial location. For the case of zero rotational speed of the turbine, shown in Fig. 8, this much simplified model gave exactly the same results as the model of Section 3, namely the 'Rotating' curves given on both plots, as would be expected. The benefit of the simplified model is that it is relatively easy to model the detailed volute and rotor geometry more precisely, rather than the averaged geometry approach used hitherto. Thus the rotor passages were then modelled as successive divisions from the volute and the cross-sectional area of the volute was allowed to diminish with distance in the correct manner, see Fig. 11. Thus a multiplicity of different parallel acoustic paths are formed between the volute and the diffuser. It is well known that if an acoustic wave is split between two parallel acoustic paths of different length and then re-combined, a system of resonances is formed due to wave cancellation at specific frequencies, the so-called Herschel–Quincke tube effect [18]. As anticipated, the model used here with its multiplicity of parallel acoustic paths through the rotor passages gave rise to a complex system of high-frequency resonance peaks due to this Herschel–Quincke interference effect. However, the low-frequency prediction up to 1500 Hz was poor in comparison to the experimental results and to that of the results from the averaged volute/rotor geometry. It proved necessary to combine the averaged and distributed models of the geometry such that the sound was deemed to propagate along a conical pipe representing half the volute before it began to diverge down the separate rotor passages. It is as though the incoming acoustic pulse first expands into the volume of the volute and then successively divides off along the rotor passages. The results from this model are shown as curves 'Volume' in the plots of Figs. 8–10.

The frequency of the resonance peaks are extremely sensitive to the input data, for instance a change in rotor length of 1 mm causes the resonant frequency to shift by 50 Hz. The acoustic length of a rotor passage is particularly difficult to quantify, due both to the tortuous axial route of the assumed 1-D propagation and to the imprecise end corrections. Thus an estimate of this length was made together with an error tolerance. All other dimensions were kept constant as they were easier to measure and hence subject to less error. The acoustic length of the rotor was then varied within the band of tolerance to see if the frequency of the first resonance peak in the direct test could be correctly predicted. This indeed was found to be the case and the rotor length was then kept constant for the inverse test and indeed all subsequent results. It is seen from the result for the reverse test that the resonant frequency is predicted reasonably well, although of course not as accurately as in the direct test, for which the rotor length was tuned.

It is seen from Fig. 8 that the interference effect between the various rotor passages provides a convincing explanation of the high-frequency resonances observed in the experimental results. Indeed the 'Volume' model that includes this effect correctly predicts the level of transmission loss at all frequencies lower than the first resonance, thereby extending the frequency range for accurate analysis quite considerably beyond that of the

'averaged' model. It is accepted that the tuning of the rotor length to give the correct resonant frequency is a luxury that in the normal modelling environment is not possible. For that reason this form of model is presented simply to reinforce the hypothesis that the high-frequency resonances are due to the Herschel–Quincke interference effect. However even if the acoustic length of the rotor passage is known imprecisely, such that the resonant frequency is subject to considerable error, the low-frequency range over which the transmission loss is calculated accurately is still extended beyond that of the averaged model.

As noted earlier, for a stationary turbine the simplified static model of the averaged geometry turbine gave precisely the same transmission loss as the 'Rotating' model of Section 3, as would be expected. It was also found that, even at turbine rotational speeds of 28,000 and 54,000 rev/min, the difference between the results from the simplified static model and the full model of Section 3 is so slight that the former results would be barely distinguishable from the latter, if they were to be drawn in Figs. 9 and 10. However, as also noted earlier, these rotational speeds are much lower than the typical turbine speeds in normal operation and the difference between results from the static and full models increases with rotational speed. Thus the full model of Section 3 should be preferred for modelling a turbine in normal operation, although a simple model of the averaged geometry of a static turbine will still give a reasonable approximation to its passive acoustic characteristics at low frequencies. Furthermore, it must be recalled that both the static and full models use the variation of background fluid properties as given by the nonlinear steady-flow analysis of Section 3.1 and the resultant convective effect of the mean flow. The Mach number changes appreciably through the turbine and peaks at the outlet of the diffuser. The peak values of Mach number are 0.18 and 0.36 for rotational speeds of 28,000 and 54,000 respectively. The variation of background fluid properties as given by the nonlinear steady-flow analysis and the convective effect of the mean flow through the turbine is quite significant especially at the higher rotational speeds of conventional operation [15].

As further evidence that rotational effects are very small at moderate turbine speeds, 'Volume' results from the static model of a distributed geometry volute and rotor are shown in Figs. 9 and 10 for turbine speeds of 28,000 and 54,000 rev/min, respectively. The accuracy with which the frequency of the lowest resonance peaks are again predicted gives further convincing evidence that they are indeed due to the interference effect. Furthermore this mechanism presents a rational explanation for the observed tendency of the experimental results to become increasingly erratic as turbine speed increases, especially near the resonant frequencies, since the change of position of a moving rotor with time presents the incoming sound wave with changing path lengths to the entry point of each rotor passage. Since the resonant frequencies are so sensitive to path length, measurement over a finite time span will include a multiplicity of resonant frequencies around the average one.

5. Conclusions

An experimental technique using an impulse test rig has been devised to enable the passive acoustic effect of the turbine of an automotive turbocharger to be characterised whilst operating under realistic conditions. A nonlinear fluid mechanical model of the turbine has been utilised to give theoretical values of the background mean flow which are of acceptable accuracy for acoustic calculations. This model was then further developed to give a linear convected acoustic model of wave propagation through a rotating turbine. The predicted results for transmission loss given by this model are in good agreement with the experimental results at low frequencies, but nevertheless at frequencies well beyond the typical cut-on frequency of non-planar propagation in an exhaust system. Thus this model is perfectly adequate to characterise the acoustic effect of the turbine within a linear plane-wave frequency domain analysis of an entire exhaust system. The model makes use of an averaged geometry of the turbine, whereby all rotor passages are lumped together into a single equivalent section.

The rotation of the turbine has minimal effect upon acoustic propagation through the turbine at the turbine speeds used in the measurements on the impulse rig. Thus a simplified static model of the turbine also gave accurate results for low-frequency transmission loss. Furthermore, the static model is simple enough for the volute and rotor to be modelled as a distributed system with distinct rotor passages. This was done and high-frequency resonant peaks in the experimental results were reproduced and attributed to interference effects due to different path lengths between the separate rotor passages. This model also extended the frequency range for accurate prediction of insertion loss. In normal on-engine operation, the turbine speed would be

about twice the highest achieved in the impulse rig test. It is recommended to retain the full model which includes rotational effects at such speeds.

Acknowledgements

The work presented in this paper was supported by the EC-project ARTEMIS (GRD-2000-25507).

References

[1] H. Chen, I. Hakeem, R.F. Martínez-Botas, Modelling of a turbocharger turbine under pulsating inlet conditions, *Proceedings of the Institution of Mechanical Engineers Part A—Journal of Power and Energy* 210 (5) (1996) 397–408.
[2] M. Abidat, M. Hachemi, M.K. Hamidou, N.C. Baines, Prediction of the steady and non-steady flow performance of a highly loaded mixed flow turbine, *Proceedings of the Institution of Mechanical Engineers Part A—Journal of Power and Energy* 212 (3) (1998) 173–184.
[3] F. Payri, J. Benajes, M. Reyes, Modelling of supercharger turbines in internal-combustion diesel engines, *International Journal of Mechanical Sciences* 38 (1995) 853–869.
[4] H. Yoshiki, N. Miyauchi, One-dimensional passage modeling of a radial turbine on the basis of design specifications, *Proceedings of the Institution of Mechanical Engineers Turbocharging and Turbochargers*, 7–9 June 1994, Paper C484/033/94, 1994.
[5] T. Kreuz-Ihli, D. Filsinger, A. Shulz, S. Wittig, Numerical and experimental study of unsteady flow field and vibration in radial inflow turbines, *Journal of Turbomachinery* 122 (2000) 247–254.
[6] S.A. Nelson, Z.S. Filipi, D.N. Assanis, The use of neural nets for matching fixed or variable geometry compressors with diesel engines, *Journal of Engineering for Gas Turbines and Power* 125 (2003) 572–579.
[7] R.J. Alfredson, P.O.A.L. Davies, Performance of exhaust silencer components, *Journal of Sound and Vibration* 15 (2) (1971) 175–196.
[8] M.L. Munjal, *Acoustics of Ducts and Mufflers*, Wiley-Interscience, New York, 1987.
[9] K. S. Peat, LAMPS software for the acoustic analysis of silencers, *Proceedings of EuroNoise*, 1995, pp. 791–796.
[10] F. Payri, J.M. Desantes, A. Broatch, Modified impulse method for the measurement of the frequency response of acoustic filters to weakly nonlinear transient excitations, *Journal of the Acoustical Society of America* 107 (2) (2000) 731–738.
[11] G.F. Mucklow, A.J. Wilson, The attenuation and reflection of compression waves propagated in pipes, *Proceedings of the Institution of Mechanical Engineers* 169 (1955) 69–80.
[12] C.L. Morfey, Sound generation and transmission in ducts with flow, *Journal of Sound and Vibration* 14 (1971) 37–55.
[13] P.H. Oosthuizen, W.E. Carscallen, *Compressible Fluid Flow*, McGraw-Hill, New York, 1997.
[14] W.J. Duncan, A.S. Thom, A.D. Young, *Mechanics of Fluids*, second ed., Edward Arnold, London, 1970.
[15] K.S. Peat, M. Elsari, S. Dequand, A linear acoustic model of the passive effect of the turbine of an automotive turbocharger, *Proceedings of the Tenth International Congress on Sound and Vibration*, Stockholm, Sweden, 2003.
[16] M.G. Prasad, M.J. Crocker, On the measurement of the internal source impedance of a multi-cylinder engine exhaust system, *Journal of Sound and Vibration* 90 (1983) 479–508.
[17] K.S. Peat, A note on one-dimensional acoustic elements, *Journal of Sound and Vibration* 88 (1983) 572–575.
[18] G.W. Stewart, The theory of the Herschel–Quincke tube, *Physical Review* 31 (1928) 696–698.